Mon. Not. R. Astron. Soc. **384,** 849–862 (2008) doi:10.1111/j.1365-2966.2007.12599.x

The eccentric accretion disc of the black hole A0620−00⋆

J. Neilsen,[1]† D. Steeghs[2,3]† and S. D. Vrtilek[2]†

[1]*Harvard University Department of Astronomy, 60 Garden Street, MS-10 Cambridge, MA 02138, USA*
[2]*Smithsonian Astrophysical Observatory, 60 Garden Street, Cambridge, MA 02138, USA*
[3]*Department of Physics, University of Warwick, Coventry CV4 7AL*

Accepted 2007 October 16. Received 2007 October 15; in original form 2007 June 19

ABSTRACT

We present spectroscopic observations of the quiescent black hole binary A0620−00 with the 6.5-m Magellan Clay telescope at Las Campanas Observatory. We measure absorption-line radial velocities of the secondary and make the most precise determination to date ($K_2 = 435.4 \pm 0.5\,\mathrm{km\,s^{-1}}$). By fitting the rotational broadening of the secondary, we refine the mass ratio to $q = 0.060 \pm 0.004$; these results, combined with the orbital period, imply a minimum mass for the compact object of $3.10 \pm 0.04\,\mathrm{M_\odot}$. Although quiescence implies little accretion activity, we find that the disc contributes 56 ± 7 per cent of the light in *B* and *V*, and is subject to significant flickering. Doppler maps of the Balmer lines reveal bright emission from the gas stream-disc impact point and unusual crescent-shaped features. We also find that the disc centre of symmetry does not coincide with the predicted black hole velocity. By comparison with smoothed particle hydrodynamics (SPH) simulations, we identify this source with an eccentric disc. With high signal-to-noise ratio (S/N), we pursue modulation tomography of Hα and find that the aforementioned bright regions are strongly modulated at the orbital period. We interpret this modulation in the context of disc precession, and discuss cases for the accretion disc evolution.

Key words: accretion, accretion discs – binaries: close – stars: individual: A0620−00.

1 INTRODUCTION

A0620−00 (V616 Mon) is the prototype soft X-ray transient, a class of low-mass binary stars which exhibit infrequent but intense X-ray bursts (Gelino, Harrison & Orosz 2001). In 1975 it became the brightest X-ray nova ever detected, at approximately 50 Crab (Elvis et al. 1975), and it was the first nova to be identified with a black hole primary (McClintock & Remillard 1986, hereafter MR86). MR86 measured an orbital period of 7.75 h and a radial velocity semi-amplitude for the K-type secondary of $457\,\mathrm{km\,s^{-1}}$, leading to a mass function $f(M) = 3.18\,\mathrm{M_\odot}$; estimates of K_2 and $f(M)$ have decreased slightly since then (i.e. $433\,\mathrm{km\,s^{-1}}$ and $3.09\,\mathrm{M_\odot}$; Marsh, Robinson & Wood 1994, hereafter MRW94). Given this minimum mass, it is likely that A0620−00 is a black hole.

A substantial amount of work has gone into the analysis of A0620−00 in the last 20 yr, with particular emphasis on ellipsoidal variations in the light curve and the contamination of the K-star flux by light from the accretion disc. As yet, no real consensus has been reached, mostly due to the complexity of the light curves. While ellipsoidal variations are obvious, they are highly asymmetric (Leibowitz, Hemar & Orio 1998); the origin of the asymmetry is undetermined. Modelling this light curve, Gelino et al. (2001) determined an inclination of $41^\circ \pm 3^\circ$, invoking star-spots to explain the asymmetries. Shahbaz, Naylor & Charles (1994) found a 90 per cent confidence interval of $i = 30^\circ$–45° given the mass ratio of A0620−00, modelling their asymmetries with the bright spot where the accretion stream hits the disc.

Light-curve modelling is also complicated by the variability of the disc itself. To quantify ellipsoidal variations, most authors assume the disc to be constant, and justify the claim by noting that A0620−00 is quiescent. They do not mention that estimates of the disc contamination range from <3 per cent (Gelino et al. 2001) to $\lesssim$50 per cent (MR86). The contribution from this disc is not only unclear but also apparently not constant. More than half of A0620−00's 58-yr burst cycle has passed, and it is important to note that quiescent does not mean inactive. We will argue that the variability of the accretion disc cannot be neglected. In order to determine definitively the mass of the compact object, it is very important to understand the structure and variation of the accretion disc. MRW94 made enormous progress towards this goal. In 2004, Shahbaz et al. (2004, hereafter S04) noticed signatures of an eccentric disc not seen in previous Doppler maps, but lacked the phase coverage to verify their hypothesis.

⋆This paper includes data gathered with the 6.5-m Magellan telescope located at Las Campanas Observatory, Chile.

†E-mail: jneilsen@cfa.harvard.edu (JN); dsteeghs@cfa.harvard.edu (DS); svrtilek@cfa.harvard.edu (SDV)

Therefore, as follow-up to the work of MRW94 and S04, and as part of a Doppler imaging survey of black hole and neutron star binaries, we undertook phase-resolved optical spectroscopy of A0620−00. In Section 2 we describe our observational methods and data reduction. In Section 3 we measure the radial velocity of the secondary star, the system mass ratio and attempt to quantify flickering. In Section 4 we present Doppler images of the accretion disc at several wavelengths, investigate evidence for an eccentric disc and report results of modulation tomography of the Hα line. We discuss conclusions from the variability of the disc and our Doppler maps in Section 5.

2 OBSERVATIONS

We observed A0620−00 with the Low-Dispersion Survey Spectrograph 3 (LDSS3) at the *f*/4 focus of the 6.5-m Clay telescope at Las Campanas Observatory on 2006 December 14–16. We acquired 48 spectra using the volume phase holographic (VPH) blue grism and a long 0.75-arcsec slit. By shifting the slit 4° redward, we were able to observe Hα with the superior resolution of the Blue grism (2.3 Å $\equiv$ 130 km s^{-1}), covering 4250–7035 Å. To minimize the effects of atmospheric dispersion, we observed at parallactic angle. Our exposure times ranged from 420 to 1200 s, with an average of 660 s (a total of 8.81 h on the source).

Each night we observed the flux standard HILT 600 with the same instrumental set-up as A0620−00. On all nights the seeing was generally comparable to our slit width, but occasionally spiked as high as 1.8 arcsec due to wind, and slit losses prevented precise flux calibration. On 2006 December 15 we also observed two K3/K4 stars, HD 18298 and 7142, as velocity standards, again with the same optical set-up. As the secondary is constrained to be later than K3V Froning, Robinson & Bitner (2007), we expect more accurate results for HD 7142, which is listed as K3/K4III in the SIMBAD data base (HD 18298 is listed as K3IIICN). For each pointing, we obtained comparison HeNeAr arc lamp spectra after every three–seven spectra, depending on the current exposure time. We list the observations in Table 1.

We used standard Image Reduction and Analysis Facility (IRAF) routines for basic data reduction (zero-subtraction, flat-fielding and spectral extraction). We extracted our spectra in multispec format, attempting *apall*'s optimal extraction using nominal LDSS3 gain, readout noise and full-well values. The routine also performs standard extraction and generates error bars. A CCD defect running across our spectra prevented reliable fits to the spatial profile for optimal extraction, so we used the normally extracted spectra instead. This choice did not significantly degrade our signal-to-noise ratio (S/N), and should have a negligible effect on our presented results. After wavelength calibration, we passed the spectra and their errors to the software package MOLLY for cleaning and analysis.

Table 1. Observation log.

Source	Date	No. of spectra	$T_{\rm exp}$ (s)
A0620−00	2006 December 14	11	873
A0620−00	2006 December 15	23	698
A0620−00	2006 December 16	14	433
HILT 600	2006 December 14	1	20
HILT 600	2006 December 15	3	20
HILT 600	2006 December 16	3	20
HD 18298	2006 December 15	3	5
HD 7142	2006 December 15	5	5

Note. $T_{\rm exp}$ is the average exposure time for the source.

3 ANALYSIS

3.1 The spectrum of A0620−00

In Fig. 1 we present the average normalized spectrum of A0620−00. The spectrum shows a number of strong features (originating from the disc) and many relatively weak K-star absorption lines. We overplot the K-dwarf template HD 7142 for reference. We have extremely high S/N Hα and Hβ lines, both observed by MRW94, as well as lower S/N Hγ and He I 6678 Å. The non-detections of He II lines indicate the scarcity of ionizing radiation. Our Hα line is stronger relative to the continuum than in 1994 by approximately 50 per cent. This relative brightening is not surprising given the decreased fraction of light contributed by the secondary. We show a close-up of Hα in panel (a) of Fig. 2. The profile has two strong symmetric peaks. It is also interesting that our Hβ line also shows two strong peaks (as opposed to a single-peaked line seen by MRW94).

The other feature of note is located on top of the interstellar sodium doublet near 5890 Å. We show a close-up of this line in panel (b) of Fig. 2. The line suffers significant extinction by interstellar sodium, so it is not possible to identify its peak unequivocally, but it seems to be He I 5875. It appears to have some structure, and trailed spectra suggest a double-peaked profile, but our attempts to correct

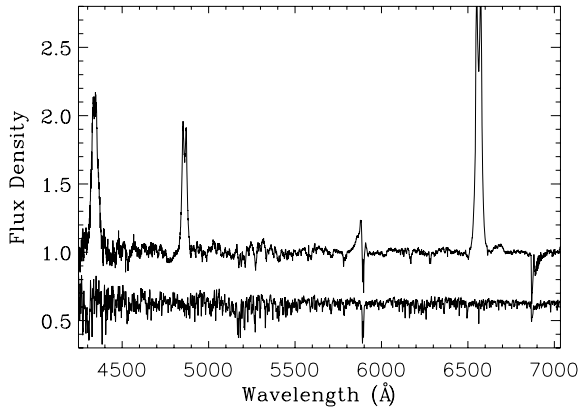

Figure 1. The average normalized spectrum of A0620−00. The strongest features are, in order of increasing wavelength, Hγ, Hβ, He I 5875, Hα, He II 6678 and telluric absorption lines. We also show the scaled spectrum of HD 7142 for reference.

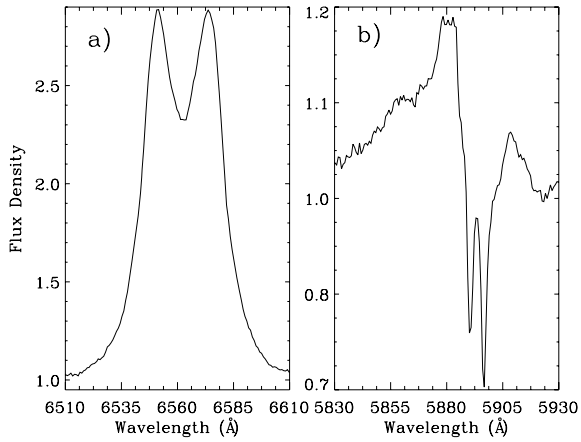

Figure 2. Close-ups of (a) the Hα line and (b) the feature near 5890 Å. Intensities are as in Fig. 1.

Table 2. Fits to rotational broadening and radial velocities.

Template	ε	$v \sin i$ (km s^{-1}) ± 2	f ± 0.001	K_2 (km s^{-1}) ± 0.4	$t_0 - 245\,4084$ $\pm$4E-5	γ (km s^{-1}) ± 8	q ± 0.004	$f(M_1)$ ($M_\odot$) ± 0.03	χ^2
HD 18298	0.45	77	0.441	435.8	0.69487	11	0.051	3.06	1.06
	0.55	78	0.441	435.8	0.69487	11	0.052	3.07	1.06
	0.65	80	0.440	435.8	0.69487	11	0.057	3.09	1.05
	0.75	80	0.441	435.8	0.69487	11	0.056	3.09	1.06
	0.85	81	0.441	435.8	0.69487	11	0.058	3.10	1.06
HD 7142	0.45	80	0.433	435.0	0.69484	−9	0.056	3.07	1.03
	0.55	80	0.433	435.0	0.69484	−9	0.057	3.08	1.03
	0.65	83	0.449	434.9	0.69484	−9	0.063	3.11	1.02
	0.75	83	0.433	435.0	0.69484	−9	0.061	3.10	1.03
	0.85	84	0.433	435.0	0.69484	−9	0.064	3.12	1.03

for interstellar absorption and create a Doppler map (Section 4) were unsuccessful.

3.2 The radial velocity of the secondary star

Following MRW94, we first measure the radial velocity of V616 Mon in order to estimate the mass function. Masking out emission lines, telluric absorption and interstellar sodium lines in our velocity standards, and normalizing, we cross-correlated our spectra against these K-dwarf templates. The results of the following sections are presented in Table 2.

As discussed in MRW94, this process requires several adjustments for A0620−00: rotational broadening and orbital smearing. The following analysis was completed for each template. We performed a preliminary broadening of the template with MRW94's value of $v \sin i = 83$ km s^{-1}. Then, after cross-correlating, we shifted our spectra into the rest frame of the template, which is essentially the rest frame of the secondary. We made 48 copies of the template and smeared each according to the formula $s = 2\pi V_i T_i / P$, where P is the orbital period and V_i and T_i are the radial velocity and exposure time for the ith A0620−00 spectrum. With exposure times of up to 1200 s, it is necessary to correct for smearing because s is comparable to $v \sin i$. We averaged the smeared templates, rotationally broadened the result with a value between 30 and 135 km s^{-1}, and optimally subtracted the final template from the average object spectrum. We assume a limb-darkening coefficient ε of 0.65 (Wade & Rucinski 1985, and references therein), but perform these calculations for $\varepsilon = 0.45$–0.85 to evaluate our systematics. The optimal subtraction routine returns the fraction f of light contributed by the secondary and a χ^2 value. We fit fourth-order polynomials to χ^2 to identify the appropriate f and $v \sin i$. Results are included in Table 2.

The measured rotational broadening of V616 Mon (80 ± 2 for HD 18298 and 83 ± 2 for HD 7142) is consistent with MRW94, but f is not, even though f and $v \sin i$ were strongly correlated (i.e. we were able to identify them with the same χ^2 minimum). MRW94 found that the secondary contributes ∼94 per cent of the light near Hα and ∼85 per cent of the light near Hβ. We observed both wavelengths simultaneously, and find that the secondary contributes only 44 per cent of the light in B and V (near 5500 Å). This conclusion is effectively independent of the limb-darkening coefficient. We will discuss systematic uncertainties on f in Section 3.4.

Finally, we performed another cross-correlation of our spectra against the template, this time with the appropriate value of $v \sin i$. The results are shown in Fig. 3. Although we took arc exposures frequently to minimize the effects of flexure, we found arc scales to drift by ∼0.5 Å over the course of a few hours. As our dispersion (0.69 Å pixel^{-1}) corresponds to 37.9 km s^{-1} pixel^{-1}, it was necessary to compensate for arc drift. We did this by cross-correlating the telluric lines near 6900 Å and shifting out the resulting velocities (generally around 10 km s^{-1}). In this way we guaranteed a common (heliocentric) rest frame for all 48 spectra.

We fit a function of the form $V = K_2 \sin[2\pi (t - t_0)/P] + \gamma$ for each template. γ represents the systemic velocity in the template frame. Although we have very high S/N, the baseline (∼seven orbits) was insufficient to make a reliable independent determination of the orbital period, so we fixed P according to the ephemeris of MR86. To get an accurate measure of our statistical uncertainties, we performed 10 000 Monte Carlo simulations for each fit, assuming each radial velocity to be distributed normally around the measured value, increasing the errors from cross-correlation by a factor of 3. For our final values, we averaged the results from both templates and took the standard deviation of the combined distribution as the uncertainty. The resulting uncertainty is not purely statistical, as the use of multiple templates includes some systematic errors (e.g. template mismatch). These results can be found in Table 2.

All fits are comparable in quality and have excellent χ^2. We find consistent values for K_2 and excellent agreement in t_0 – we observed inferior conjunction on the second night – and our measurements are independent of limb darkening ($\varepsilon = 0.65$ is marginally preferred). We will consider the systemic velocities only briefly. The uncertainties in γ are dominated by the systematic uncertainty (one fifth of a pixel, or ∼7.6 km s^{-1}). We were unable to find a catalogued radial velocity for HD 18298, but from Malaroda, Levato & Galliani (2001), the radial velocity of HD 7142 is 32.8 km s^{-1}. Given that MRW94 report a systemic velocity of 22 km s^{-1}, we consider these fits to be accurate; the choice of template does not significantly affect K_2, t_0 or $v \sin i$. In summary, we adopt $v \sin i = 82 \pm 2$ and $K_2 = 435.4 \pm 0.5$ km s^{-1}. In addition, we find that inferior conjunction of the mass donor star, which defines the zero-point t_0 of our ephemeris, occurs at HJD (UTC) 245 4084.69485 ± 0.00005. This latest t_0 is consistent with the ephemeris of MR86 (within 0.5σ).

3.3 The mass ratio

To measure the mass ratio, we use Paczynski's (1971) formula relating the rotational broadening and K_2 to q for Roche lobe filling stars:

$$\frac{v \sin i}{K_2} = 0.462[(1+q)^2 q]^{1/3}. \quad (1)$$

This gives $q = 0.060 \pm 0.004$, where the uncertainty includes variation between templates. This value is consistent with MRW94's

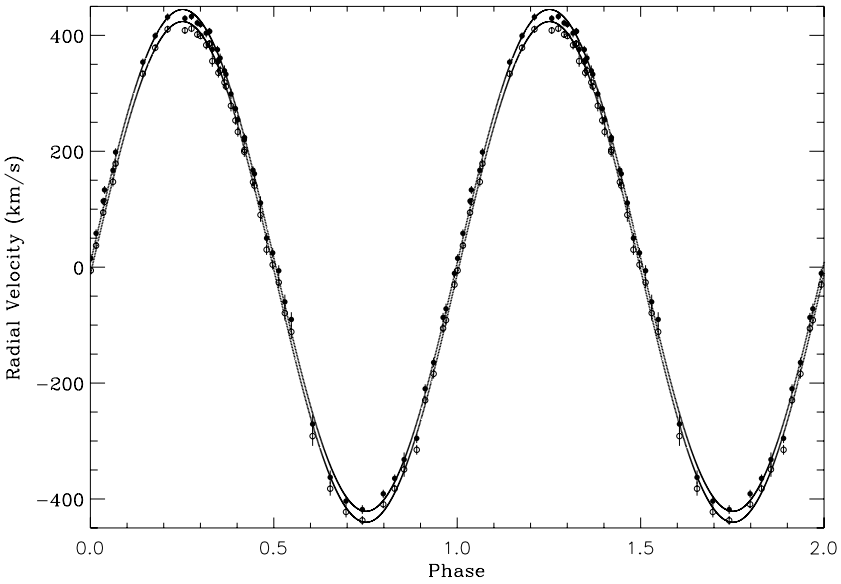

Figure 3. Radial velocity of V616 Mon. Two cycles are shown for clarity. Filled circles correspond to the template HD 18298, and open circles to HD 7142. Note from Table 2 that the main difference is in γ.

measurement (by the same method) of 0.064 ± 0.01, and with their value of $q = 0.067 \pm 0.01$, obtained by calculating models on a grid over the Roche lobe, including gravity darkening and quadratic limb darkening. Although it might be possible with our improved resolution to distinguish between the Paczynski approximation and the grid models, since the grid model correction was far from significant at their 1σ level, we opt to take our results as accurate. This choice is validated by the weak (at best) dependence of our measurements on limb darkening, and we report uncertainties large enough to account for any systematics in ε.

Given the orbital period, K_2, and q, the minimum masses for both objects are

$$f(M_1) = 3.10 \pm 0.04\,\mathrm{M}_\odot,$$
$$f(M_2) = 0.19 \pm 0.02\,\mathrm{M}_\odot,$$

where the true mass goes like $M_{\rm min}/\sin^3 i$. As noted in many papers (MRW94; Shahbaz et al. 1994), the mass of a maximally rotating neutron star with the stiffest equation of state is $3.2\,\mathrm{M}_\odot$; if causality is the only constraint, the absolute upper limit is $3.76\,\mathrm{M}_\odot$ (Friedman & Ipser 1987). Using the constraints $39^\circ \leqslant i \leqslant 75^\circ$ (Gelino et al. 2001), we find $3.4 \leqslant M_1 \leqslant 12.6\,\mathrm{M}_\odot$, with the most likely value at $11.1\,\mathrm{M}_\odot$. We thus improve the precision of the mass function, but it remains a possibility that A0620−00 is a stiff, massive neutron star.

3.4 Ellipsoidal variations and the variability of the disc

Part of the difficulty in measuring the parameters of A0620−00, and a possible source of systematic error, is the tidal distortion of the secondary. We assume, for example, in our radial velocity measurements, that the secondary's centre of light coincides with its centre of mass. For a star filling its Roche lobe with some gravitational and limb darkening, this assumption is not likely to be valid. Following Sterne (1941), we checked for this distortion in our data by fitting an extra $-\,K_{\rm ell}\sin(4\pi\phi)$ term to our radial velocity curve. Orbital elements from Gelino et al. (2001) lead to a predicted $K_{\rm ell} = 3.0\,\mathrm{km\,s^{-1}}$, but we found $K_{\rm ell} \sim 0.7\,\mathrm{km\,s^{-1}}$ (less than the error bars on each radial velocity), and an insignificant improvement to χ^2. It is possible that our data have insufficient S/N to make this measurement. This particular effect is small, but we must be careful not to dismiss the systematic uncertainties from ellipsoidal effects.

Ellipsoidal variations, particularly in the light curve, receive a great deal of attention because of the constraints they place on the orbital parameters, especially the inclination. In practice, one usually attributes all variation to the secondary (assuming the disc to be constant). However, the fact that the fraction of light contributed by the disc changes by a factor of 9 over 10 yr casts significant doubt on that particular assumption. In turn, this evolution must be accounted for when interpreting light curves spanning a long period of time.

Given that we have good spectral resolution and relatively good phase coverage, we have attempted to characterize the ellipsoidal variations of the source during our observations. While it is most common to address variations in the light curve, effects of tidal distortion should also be apparent in the secondary light fraction and the line equivalent widths. In the rest of this section we quantify these variations.

If the disc is a constant diluting source of light, then continuum variations, and therefore variations in the equivalent widths of lines, maybe be attributed to the tidal distortion of the secondary. In Fig. 4(a) we show the equivalent width of the Hα line as a function of orbital phase. The asymmetric ellipsoidal variations observed by Gelino et al. (2001) are obvious, along with noticeable scatter. Given a S/N of ∼95 at Hα, it seems reasonable to interpret this as flickering, albeit undersampled, rather than noise. We will discuss the equivalent widths in more detail shortly.

Fig. 4(b) shows the secondary light fraction f as a function of orbital phase. We can evaluate the variability of the disc with a back-of-the-envelope calculation of $f(\phi)$. We assume the secondary continues to exhibit ellipsoidal variations of 0.077 mag (MRW94 using $i = 40^\circ$), or flux variations of 7 per cent, and that the disc is constant in time. Since the disc contributes 56 per cent of the light, it should be roughly 22 per cent brighter than the secondary. Then in units of the mean secondary flux, $F_2 = 1 - 0.07\cos(4\pi\phi)$ and $F_1 = 1.22$, and

$$f = \frac{1 - 0.07\cos(4\pi\phi)}{2.22 - 0.07\cos(4\pi\phi)}. \quad (2)$$

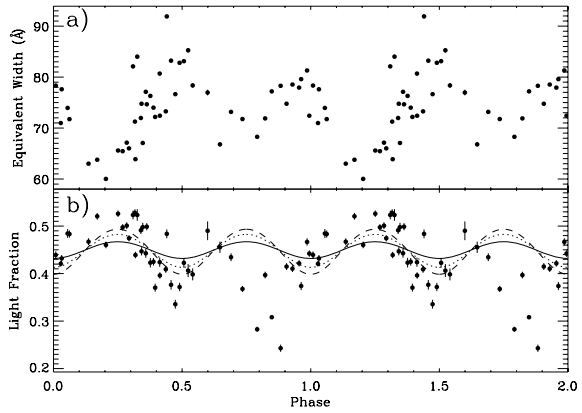

Figure 4. (a) Equivalent width of the Hα line. (b) Secondary light fraction as measured from 5000–5800 and 6000–6500 Å for the template HD 7142. Differences from HD 18298 are less than 1σ. These plots indicate a flickering source of light. The solid, dotted and dashed lines are the predicted light fraction for a constant disc and ellipsoidal modulations, for inclinations of 40°, 60° and 80°, respectively. See equation (2).

The inclination-dependent amplitude of ellipsoidal variations is tabulated in MRW94. Equation (2) is plotted along with f for inclinations of 40°, 60° and 80°. We have matched the mean relatively well, and to some extent the functional form, but it is obvious that our assumptions do not hold. First, the disc appears anomalously bright between $\phi = 0.7$–0.9. As this phase interval was observed on the second night only, we cannot speculate if the dip in f indicates a flare or a long-lived bright region of the disc, like a warp, visible only at this phase.

The second and more troubling discrepancy is the large amplitude of variation of f. As is apparent from Fig. 4(b), excluding $\phi = 0.7$–0.9, higher inclinations are preferred, even those which are ruled out by the lack of eclipses in this source. Accepting momentarily the inclination determined by Gelino et al. (2001), this figure illustrates very clearly the significance of the assumption that the disc is a constant source of light; by requiring a constant disc, we could overestimate the inclination by several tens of degrees. Now it is reasonable to assume that the secondary has not evolved substantially in the last 20 yr, so we must conclude that the discrepancy between the predicted and observed light fractions is related to activity in the disc. For example, a component of disc light modulating at the orbital period could reproduce the effect easily.

Unfortunately, there is no a priori way to determine in advance the viability of an inclination measurement. Small and Moderate Aperture Research Telescope System (SMARTS) data from the last 10 yr show that A0620−00 goes through periods of quiescence, where ellipsoidal modulations are observed, and periods of erratic variability which gradually swamps the smooth component (Cantrell & Bailyn, private communication). In these active periods, the source is extremely variable on time-scales from minutes (our observations) to years (SMARTS), and the variability is highly phase dependent, so that ellipsoidal modulations cannot be reliably measured; the current active state has persisted since 2003 December. Associating this variability with the disc, we warn against measurements of i during such periods. We can expect, furthermore, a strong correlation between flickering and the light fraction. There is no reason f cannot be small and constant simultaneously, but an increase in light from the disc can only mean an increase in accretion activity, for which flickering is highly probable.

This is admittedly a grim assessment of the situation, but light-curve estimates of the inclination made during periods of variability or non-negligible contamination by disc light are unreliable. The variation in f itself is a final source of systematic uncertainty. We have a very precise measurement of the dilution fraction for the average spectrum, but that precision is only meaningful if f is not variable. Instead, we take the standard deviation in $f(\phi)$ as our uncertainty: $f = 44 \pm 7$ per cent, and summarize the discussion above by reminding the reader that quiescence is not inactivity, and ought not be used to justify invalid assumptions.

Consider now the equivalent width. Since the continuum varies slowly over our lines, it is trivial to show that the line equivalent width is given by

$$\mathrm{EW(\AA)} \simeq \frac{\mathrm{EW_{disc}}}{1+f}, \tag{3}$$

where $\mathrm{EW_{disc}}$ is the ratio of flux integrated over the line to the disc continuum, and f is the secondary light fraction. If the disc varies uniformly or not at all, $\mathrm{EW_{disc}}$ should be a constant for any given line. We can then attribute variations in the equivalent width to variations in f, which would be ellipsoidal in nature. However, measurements of the equivalent width with the secondary subtracted should reveal the reliability of this shaky assumption.

The equivalent width of our unsubtracted Hα line (open circles) is shown in Fig. 5; it should be compared to the same plot from MRW94. To facilitate this comparison, we have overlaid their best-fitting line. We find good agreement with their phasing and amplitude, but an increase in average equivalent width of approximately 13 Å. As noted earlier, the Hα line is brighter relative to the continuum than it was in 1994, so this increase is reasonable. Also shown in Fig. 5 (filled circles) is the equivalent width of the same line after subtraction of the secondary. To achieve this result, which indicates the magnitude of fluctuations in the disc, we normalized, broadened and smeared the template, subtracted $f(\phi)$ times the template from each spectrum, and set the continuum to one. The dip between phases 0.7 and 0.9 corresponds to the possible flare seen in the light fraction.

We also note that the subtracted modulations are in phase with the unsubtracted equivalent widths. As the secondary is expected to contribute more light at longer wavelengths, the phasing may be an artefact of improper secondary subtraction, because the strongest contributions to f come from 5000 to 5800 Å. However, this effect

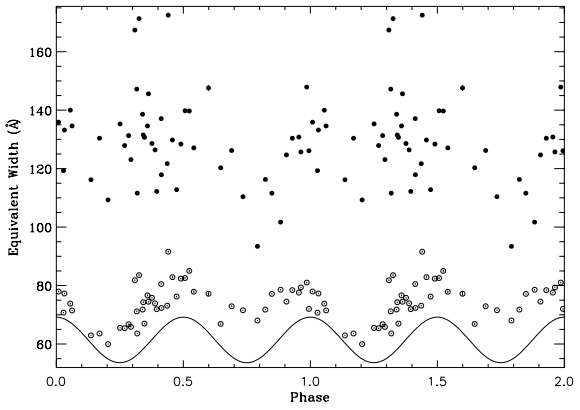

Figure 5. Measured equivalent widths for the Hα line from A0620−00. Open circles correspond to unsubtracted spectra; filled circles were calculated after subtracting the template HD 7142. Again, differences between templates were insignificant, and the errors are smaller than the circles because of the extreme S/N. We have plotted MRW94's best fit for comparison.

should be small because absorption lines up to 6500 Å were used in the measurement. Even if this is the case, the scatter in EW_{disc} cannot be explained by the combined noise in f and EW. We suggest that the most probable extra source of scatter is physical variability of the disc, i.e. flickering. In this case, the fact that the subtracted equivalent width is not constant suggests that the disc fluctuations cannot be spatially uniform.

Our measurements of flickering are confirmed by nearly simultaneous observations with all four Infrared Array Camera (IRAC) bands on *Spitzer* and the 1.2-m Fred Lawrence Whipple Observatory (FLWO) telescope (McClintock, private communication). These observations, taken in the last week of 2006 November, show strong erratic variability which is well correlated between telescopes. Neither ellipsoidal variations nor the orbital period is obvious through these fluctuations. The conclusion is clear: the assumption that the disc is constant is not valid, though it may be a good approximation if the disc contribution to the continuum is negligible (for example, when Gelino et al. 2001 found $f \gtrsim 97$ per cent and $i = 41^\circ \pm 3^\circ$). To investigate further the spatial and temporal intensity of the disc, we present the results of Doppler tomography and modulation tomography in Section 4.

4 DOPPLER IMAGING

In this section we discuss the results of Doppler tomography of the emission lines from A0620−00. To create each image, we subtracted the scaled HD 7142 spectrum, performed a linear fit to the continuum around each line, normalized and set the surrounding continuum to zero (required by DOPPLER). MRW94 express some uncertainty as to the propriety of interpolating over the Hα line in the template spectrum. Doing so removes an image of the donor star in the map, and it is not clear which is the appropriate choice. However, we found that Doppler maps including the light from the secondary do not show donor emission, so we chose to interpolate over the line. Then we binned the spectra to a uniform velocity scale and passed them to the DOPPLER routine, which computes the maximum entropy image that reproduces the observed line profiles during the course of an orbital period. For an excellent summary of the method, see Marsh (2001).

4.1 The maps

In Figs 6–9 we present Doppler tomograms of the strong emission lines in A0620−00. In each figure, the left-hand column is, from top to bottom: the observed trailed spectrum, the Doppler map and the fitted data. The right-hand column is the observed data minus a simulated symmetric part, the asymmetric part of the Doppler map and its fitted data. In the maps, we plot the Roche lobe of the secondary, the ballistic trajectory of the gas stream (lower line), and the Keplerian velocity of the disc along the stream (upper line).

In Fig. 6 we show the maps of Hα. The most obvious feature is the bright spot, which corresponds to the gas stream impact point. As found by MRW94 and S04, in our maps the gas stream trajectory and the Keplerian disc velocity along the stream (the two lines plotted in the map panels) bracket the bright spot. We can interpret this as post-shock emission, originating somewhat inside the outer edge of the disc (Marsh et al. 1990). Using the ballistic trajectory, we locate the spot at $r = 0.6 \pm 0.05 R_{L1}$. If the disc velocities are Keplerian and the spot moves with the disc, we find the outer edge near $r = 0.45 \pm 0.05 R_{L1}$. This is some indication of our systematic uncertainties, but we shall suggest shortly that the larger disc is more likely.

The other features of note are the two crescents at ∼7 o'clock and ∼2 o'clock. We shall address their origin shortly. The fitted data are rather messy, mainly due to the presence of those features and the strong flickering. Because the crescents and the bright spot so thoroughly dominate the image, the symmetric part is too bright, and we oversubtract to make the asymmetric part. Still, we do detect some emission from the bright spot. The trail itself is not particularly sinusoidal: it is more of a zigzag than an S wave. The discrepancy is best seen in the simulated asymmetric trail (bottom right, Fig. 6), but is apparent in the top panels as well. In the data panel (top left), the trail is diagonal between $\phi = -3$ and -2.5, but nearly horizontal at $\phi = -2$. It is difficult to interpret this as the S wave of a circular orbit. If the orbit is not circular, it may be a combination of the ballistic trajectory of the stream and the motion of the disc, or it may be an elliptical orbit.

In Fig. 7 we show maps of Hβ. Again, we see the crescent features; their shape is more apparent despite the lower S/N at Hβ. For the same reason, we have less trouble computing the symmetric part, and our asymmetric part shows some emission along the stream. While the corresponding trail does look nicer than its Hα counterpart, the two seem to be consistent. In Fig. 8 we show maps of Hγ, and in Fig. 9 we show maps of He I 6678. These two maps, at much lower S/N, reveal bright spot emission with some contribution from the stream itself.

4.2 The eccentric disc of A0620−00

In the previous sections, we have presented evidence for a bright flickering disc which contributes more than half of the light from the source in the optical. It is already clear that the 'no intrinsic variability' assumption of Doppler tomography is not satisfied by A0620−00. We should therefore exercise caution in interpreting our Doppler maps. Tomography is a robust technique, but the physical relevance of its results depends on the extent to which its assumptions are violated. For example, we assume that all velocity vectors corotate with the binary. However, if the disc is large enough, it may reach an orbital resonance with the secondary and become eccentric by tidal distortions. It will then precess, even in the corotating frame. For the mass ratio of A0620−00, the dominant resonance is 3:1 (Whitehurst & King 1991). Recent smoothed particle hydrodynamics (SPH) simulations by Foulkes et al. (2004) show that the manifestations of eccentric discs are bright emission between the gas stream and the Keplerian disc velocity along the stream, non-sinusoidal S waves, crescent-shaped features in Doppler maps and the shifting of the map centre of symmetry away from $(0, -K_1)$.

S04 observed the first three features and invoked an eccentric disc, but they also point out one possible objection: MRW94 found a clean circular disc. However, we have exposure times comparable to MRW94 with a larger telescope; our higher S/N may have enabled us to detect this phenomenon. The other explanation is that the crescent was absent in 1994, and the source has changed. It is thought that A0620−00 has an outburst recurrence time of 58 yr, and more than half of that time has passed since 1975, so the system should be gearing up for a new outburst. In the disc instability model of outbursts, the disc steadily recharges between outbursts, growing in size and density until it becomes unstable. In the context of this model, it is quite possible that since 1994, we have actually watched the disc expand towards the 3:1 resonance ($r = 0.66 R_{L1}$) and become distorted. If this resonance is inside the disc, then the distortion time-scale is $q^{-2} P_{orb}$, or about 90 d (Frank et al. 2002). If not, the process is slower, but a change over 12 yr for A0620−00 seems reasonable.

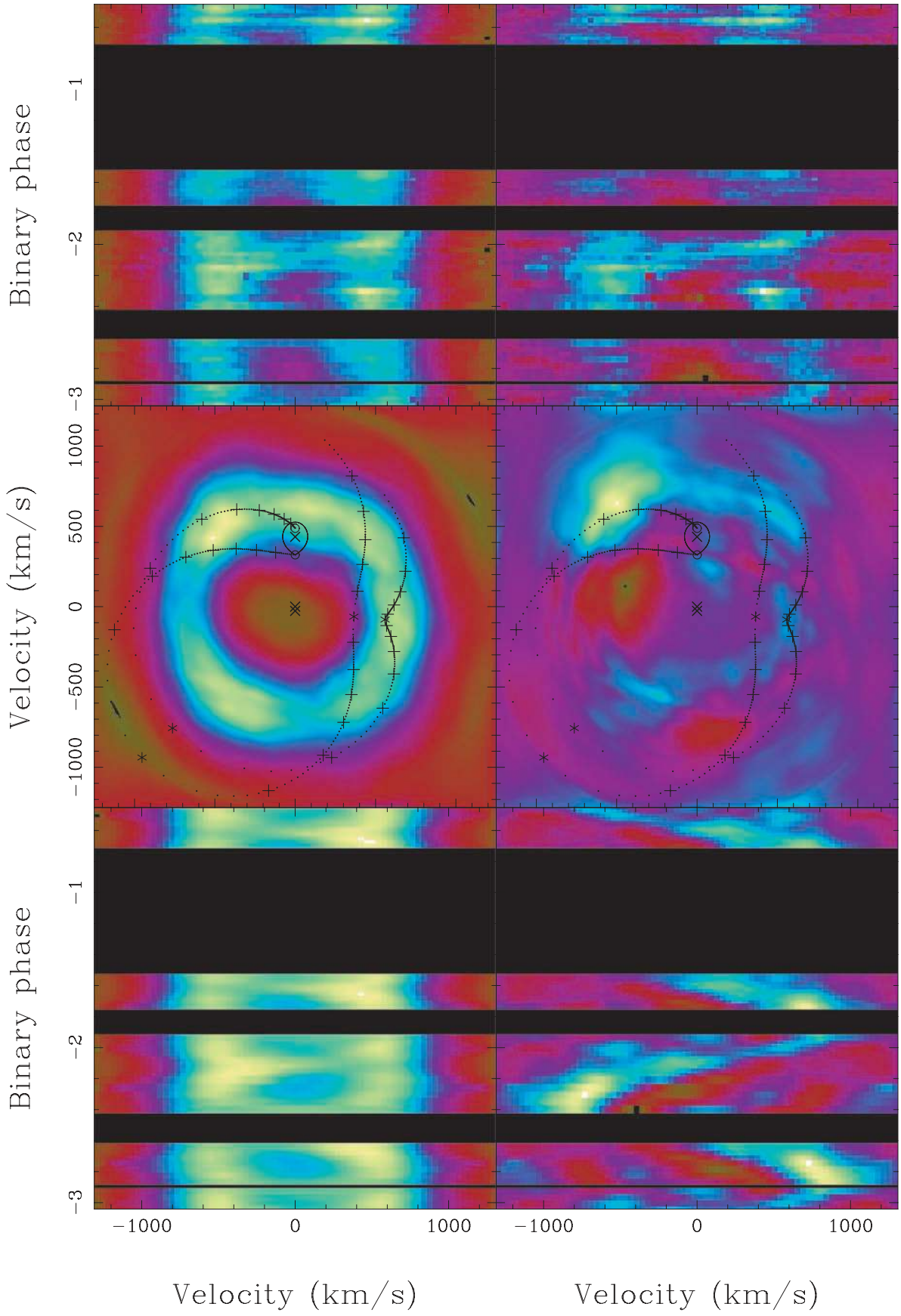

Figure 6. Hα Doppler maps. Notice in the middle left-hand panel that the bright spot is located between the gas stream trajectory and the Keplerian velocity of the disc along the stream, and the brighter crescent-shaped features.

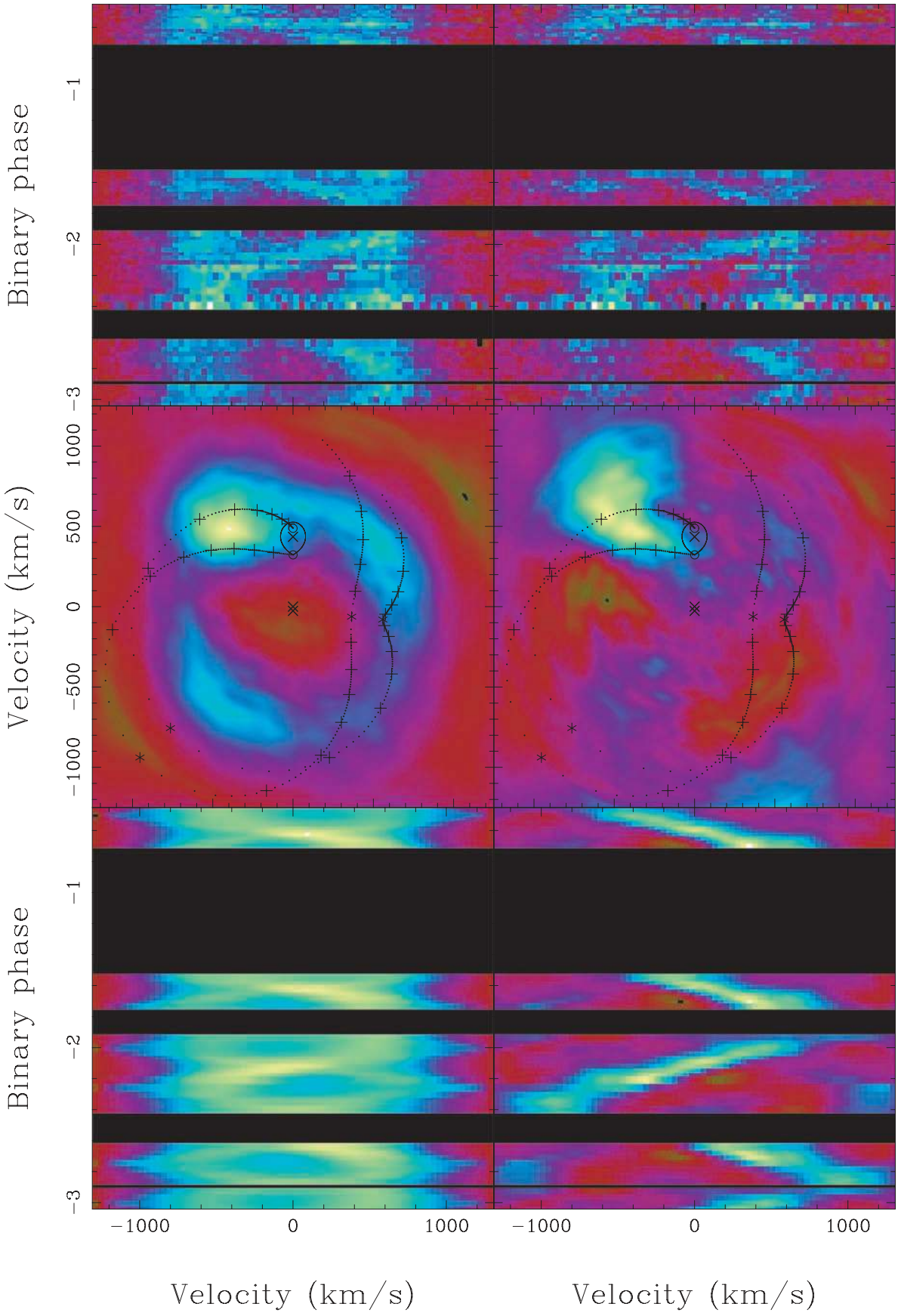

Figure 7. Hβ Doppler maps. The bright spot is again between the gas stream and the Keplerian disc velocity, and the crescents are obvious. The gas stream itself is clearly visible in the asymmetric part (middle right).

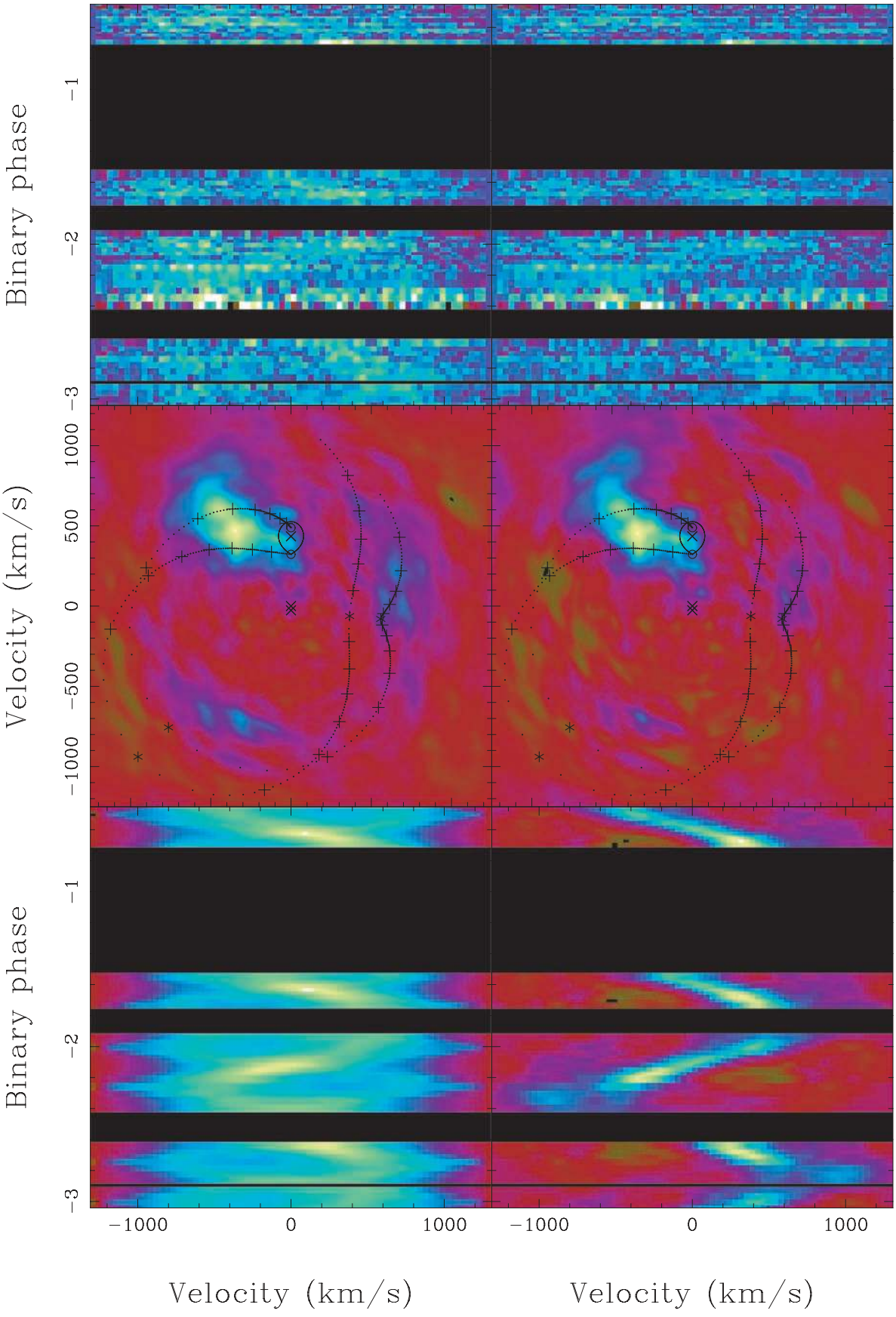

Figure 8. Hγ Doppler maps. Only the bright spot is prevalent.

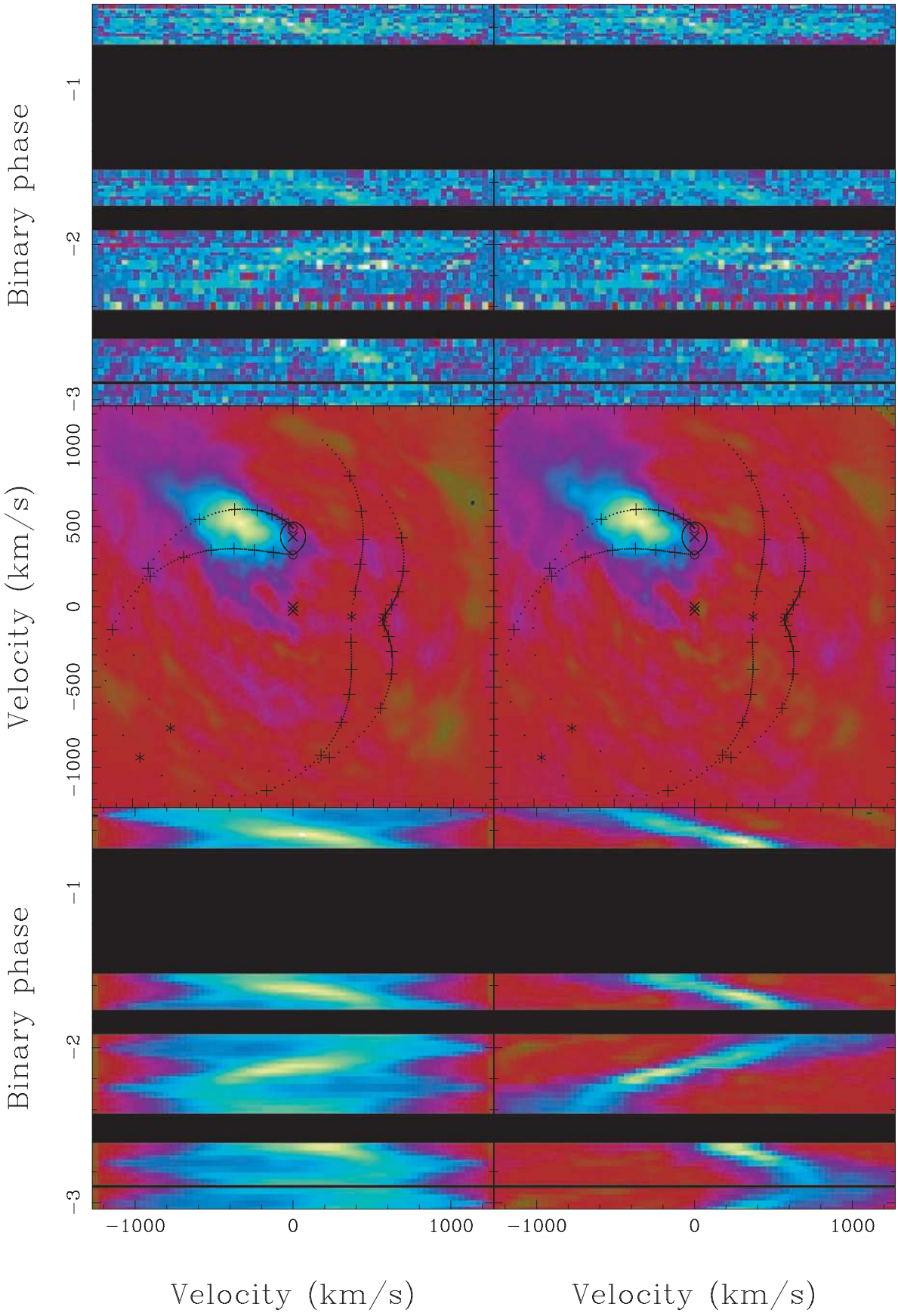

Figure 9. He I 6678 Doppler maps. Again, only the bright spot is apparent.

Now if the disc is actually circular, the Doppler map should be radially symmetric about the point $(0, -K_1)$, and by locating the centre of the disc, we can identify the radial velocity of the black hole (Steeghs & Casares 2002). Otherwise, the eccentricity of the disc should be evident in a discrepancy between the observed and predicted locations of this point. We therefore implemented a search for the disc centre of symmetry, starting at the predicted point and extending $\pm 200\,\mathrm{km\,s^{-1}}$ in V_x and V_y, subtracting the symmetric part, squaring and computing the mean and standard deviation. The point with the lowest mean corresponds to the centre of symmetry. We iterated our search, updating the centre and improving the resolution until we found the minimum.

Since our disc is very structured, it was difficult to find a region of the image unaffected by bright spots, so we performed our search on a smoothed version of the map. We then ran 10 000 Monte Carlo simulations to find the centre of symmetry, using the standard deviation of the residuals as the uncertainty to be sampled. Combining the results for our Hα and Hβ maps, we find the centre of symmetry at $(80, -220) \pm (40, 20)\,\mathrm{km\,s^{-1}}$, well outside the uncertainty in K_1. Since we cannot explain a factor of 9 of implied increase in q, we take this result, coupled with the bright spot location and the crescent features in the maps, as evidence for the non-zero eccentricity of the disc.

Finally, we recognize that as the disc precesses, its apparent centre of symmetry should move, as this point roughly corresponds to the mean radial velocity of the disc. We made Doppler images of the first night and the two halves of the second night, and performed the above search for the centre of symmetry for each. However, the low phase coverage of these maps results in large uncertainties, and we are unable to determine a trend. The feasibility of such a measurement also depends on the portion of the disc participating in eccentricity and precession, and the exact precession period, which is generally estimated at ∼30 orbits. With improved spectral resolution, a sequence of 3–4 full nights (for sufficient phase coverage per night) sampling the precession period should allow the motion of the centre of symmetry of the disc to be resolved.

4.3 Modulation tomography

It is also possible to relax the assumption of Doppler tomography that the source flux is constant throughout the orbit (Steeghs 2003). The new technique of modulation tomography allows not only the imaging of average line emission from an accretion disc but also maps harmonic variations on the orbital period. The technique is robust and flexible, but requires somewhat better S/N than standard tomographic imaging. Therefore, we only consider our Hα profile here. The process of creating modulation maps is quite similar to standard tomography, and is described in Steeghs (2003). The map is presented in Fig. 10.

It is clear from the fitted data (top right) that modulation tomography does a much better job reproducing the trail than standard Doppler mapping. Whereas standard mapping could only reach $\chi^2 = 35$, we were able to attain $\chi^2 = 9.75$ with modulation tomography. The poor χ^2 is due to flickering. The constant portion of the map (middle row, left-hand panel) looks quite similar to the maps presented in previous sections, though the bright spot is significantly smaller. We still place it off the gas stream trajectory, but it is much less diffuse, and is located, as before, near $r = 0.6R_{\mathrm{L1}}$. It is clear from this image that the inner edge of the disc in velocity space, and thus the outer edge of the disc in physical space, extends as far as $0.7R_{\mathrm{L1}}$. The crescents are not nearly as prevalent in the constant part, but are apparent in the modulation maps. The crescent placed at 7 o'clock in the standard map appears in the $\cos\phi$ map (bottom left) and the crescent placed at 2 o'clock appears in the $\sin\phi$ map (bottom right). The full modulating amplitude is shown in the middle row, right-hand panel.

For an erratic source like A0620−00, these maps must be interpreted carefully. Modulation tomography, as mentioned, maps only harmonic variations, and the demonstrated flickering is hardly harmonic. However, we have shown the eccentric disc to be a viable explanation for the observed phenomena, and the regions responsible for the crescent emission are not constant by any means. It is clear from the constant image that the inner edge of the disc in velocity space, and thus the outer edge of the disc in physical space, extends as far as $0.7R_{\mathrm{L1}}$, lending credence to the 3:1 resonance argument. For typical disc precession, superhumps are observed with periods 3–5 per cent off the orbital period (Whitehurst & King 1991). If indeed this modulating emission is caused by viscous dissipation at the outer edge of an eccentric precessing disc, there should be some power at P_{orb}, though a map of variation at some superhump period P_{sh} would reveal larger amplitudes. As yet, such a map is not possible. None the less, modulation tomography has provided yet another piece of evidence for our eccentric precessing disc model, and the fact that there is a component of disc light modulating at the orbital period could explain the observed light fraction from the secondary.

5 DISCUSSION

We have presented spectroscopic analysis of the black hole binary A0620−00. We measure an absorption-line radial velocity $K_2 = 435.4 \pm 0.5\,\mathrm{km\,s^{-1}}$. With two measurements of the rotational broadening of the secondary, we find a mass ratio of $q = 0.060 \pm 0.004$ and a minimum mass of $3.10 \pm 0.04\,\mathrm{M}_\odot$ for the primary object. With the most likely inclination of 41° from Gelino et al. (2001), measured in J, H and K, the black hole has a mass of $11.1\,\mathrm{M}_\odot$. The strong infrared flickering discussed earlier, in conjunction with unexplained smooth variability in the light curve and uncertainty in the disc spectrum itself, makes it difficult to estimate the true uncertainty in the inclination. The range of reported inclinations, 31° to 70.5° (Gelino et al. 2001, and references therein), results in a black hole mass between 3.7 and $22.7\,\mathrm{M}_\odot$. Until the nature and variability of the light from the disc is revealed in full, this conservative error estimate must be sufficient.

We also find that the secondary contributes 44 ± 7 per cent of the light near 5500 Å. As this means that the disc contributes a significant fraction of the light, especially in emission-line regions, it becomes important to assess the variability of the disc, particularly if the inclination is to be determined by light-curve modelling. As noted, it is common to assume that the disc is a constant source of light. While it may be valid when f is large, three observational points cast doubt on this assumption.

(i) S04 performed a detailed study of flares from A0620−00, which in their observations have amplitudes nearing 20 per cent of the source flux.

(ii) Measurements of the fraction f of light contributed by the secondary have not been consistent. MR86 found 40 ± 10 per cent at 5100 Å, MRW94 found 94 ± 3 per cent at Hα and Gelino et al. (2001) found $f \gtrsim 97$ per cent in J, H and K, assuming a *constant* diluting source of light.

(iii) Observations in all four *Spitzer* bands, taken approximately two weeks before our observations on the Clay telescope, show strong flickering which is highly correlated with simultaneous R-band light curves from the 1.2-m telescope on Mt. Hopkins.

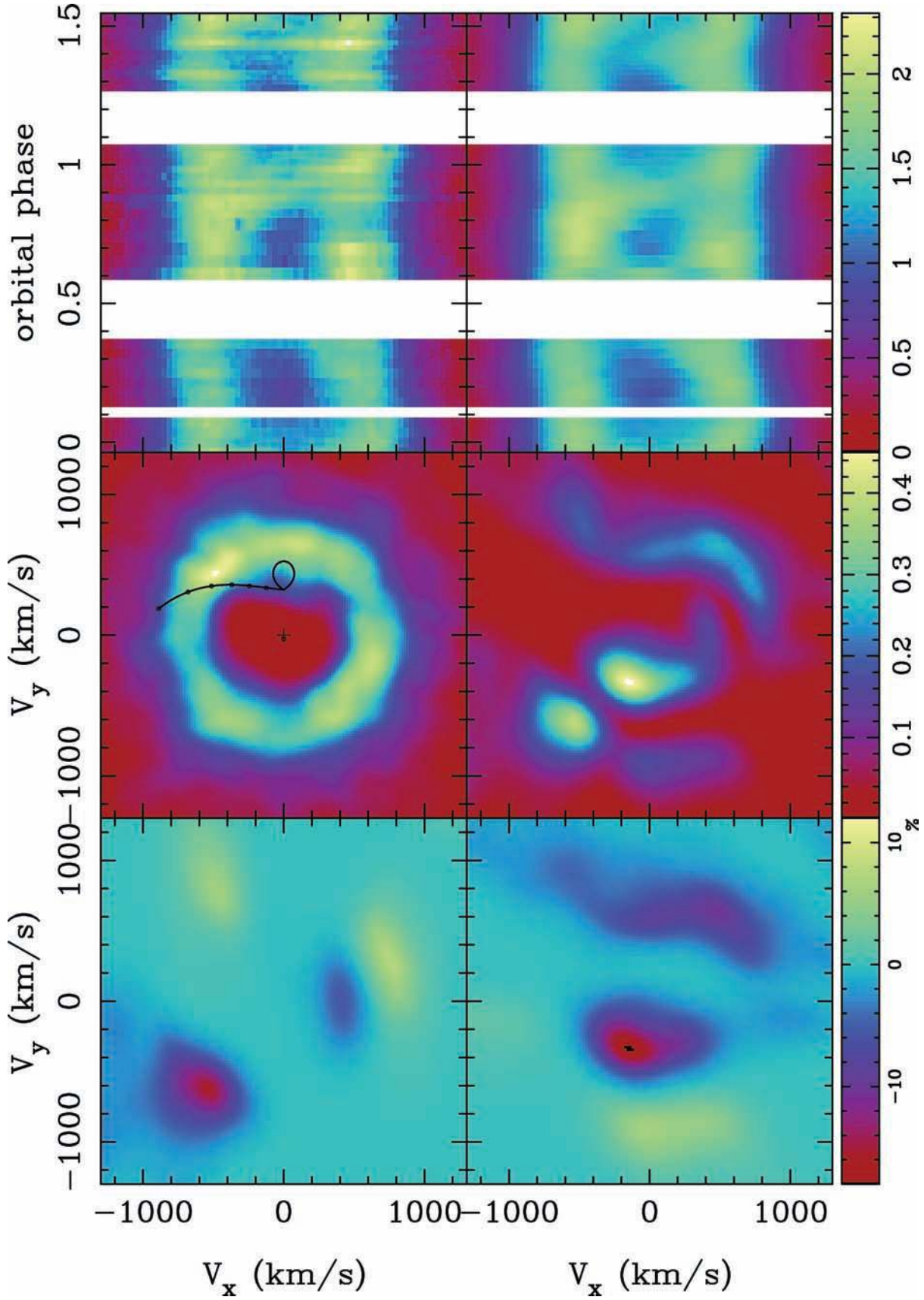

Figure 10. Hα modulation map. The observed data (top left) are well reproduced by the fitted data (top right). The middle left-hand panel shows the constant part of the disc, and the middle right-hand panel shows the amplitude of modulation. The bottom row, left and right, are the cosine and sine components of variation, respectively. The crescent regions are obviously modulated at the orbital period.

While McClintock, Horne & Remillard (1995) rightly point out that the absorption line strength of the template will affect the observed dilution fraction, unless it can be shown that the measured fraction is strongly correlated with template line strength, a physical origin for this variation cannot be ruled out. Future studies could assess the true dependence of f on template star, as well as the long-term variability of f, by observing both BS 753 (MWR94's template) and HD 7142. Our measurements of the Hα equivalent widths, when compared to those of MRW94, suggest a physically real origin for the variation, because equivalent widths are independent of the template star and the instrument. So there appears to be evidence for a disc which is brighter relative to the secondary than it used to be.

Indeed, the modulations of the equivalent width even point to a physically non-uniform flickering, because the disc emission lines vary relative to the non-stellar continuum. We can tentatively identify the flickering with the crescents, neither of which was present in 1994, so our conclusion seems viable. The line emission and the continuum may have different radial emissivity dependencies, which could result in slower modulations. We also detect several bright regions in the disc: one near the gas stream impact point, and two crescent-shaped regions on opposite sides of the disc. The reality of these features, as well as the non-uniform flickering, are confirmed by modulation tomography of the Hα disc line, which reveals variation near the bright crescents.

First noticed by S04, the crescent-like features may indicate an eccentric disc, which is predicted for systems like A0620−00 with small mass ratios and large discs. It seems that we have observed an eccentric disc, but let us consider the evidence. From our observations, the following are clear.

(i) The disc is bright and variable. The brightness is evident in the increased dilution of the secondary spectrum, and the variability is clear from a number of phenomena. First, the trailed Hα line shows clear evidence of flickering events. Second, the subtracted equivalent width of the same line is variable beyond explanation by noise alone. Third, the phase-resolved light fraction cannot be reproduced by ellipsoidal variability on top of a constant source of light.

(ii) The disc extends to the 3:1 tidal resonance. This is a simple point, clear from the Doppler and modulation maps.

(iii) The disc is not centred on the radial velocity of the black hole.

(iv) The disc is not radially symmetric, but characterized by bright crescent-shaped regions.

(v) The crescent regions are modulated at the orbital period.

Each of these points alone would be insufficient evidence to conclude that the accretion disc is eccentric and precessing. However, with the exception of a direct image of the elliptical disc, we can present a complete and coherent argument that this is the case. The disc has grown to tidal resonance, where the enhanced disc viscosity results in bright and variable rims of extra dissipation. We then observe crescents of extra dissipation at relatively low velocities, as expected. Given the viscous effects, it is predicted that the disc will receive a gravitational torque from the secondary, and begin to precess. The asymmetries introduced here shift the velocity centre of disc emission away from the black hole, and we find that the disc is not centred on the black hole in velocity space. Furthermore, given the beat period between the precession and orbital motion, the regions of viscous dissipation should be modulated at roughly the orbital period. Modulation tomography reveals this to be the case.

In retrospect, knowing that portions of the disc are modulated on the orbital period, we look closer at the fraction of light contributed by the secondary star, and see that it is not well fit by ellipsoidal modulations for a system at the inclination of A0620. However, if another component of the system was variable on the orbital period, as we have observed the disc to be, then there is no need for concern. The physical picture, a precessing elliptical disc torqued by the secondary star, predicts and produces all the phenomena we have discussed in our data, which are of high quality.

To put it another way, the eccentric disc hypothesis is nicely self-consistent. It explains why and how the accretion disc has changed, allows the disc to be large enough for the growth of eccentric modes and predicts the phenomena that we observe. It is unfortunately not possible at this point to make an estimate of the disc eccentricity. Smith et al. (2007) have shed a great deal of light on the evolution of disc eccentricity and energy dissipation with three-dimensional (3D) SPH simulations. They find that systems with q between 0.08 and 0.24 develop low-mass eccentric discs with superhumps; for $q = 0.0526$, the disc exhibits a short-lived superhump and decaying eccentricity. All mass ratios show enhanced dissipation in the disc from the thermal-tidal instability, even without the eccentric modes.

Since we have not observed a superhump, we cannot place A0620−00 in either category. If it falls in the more extreme group, the disc eccentricity is likely zero (reached after about 300 orbital periods; Smith et al. 2007). In that case, the steady state is a massive disc. If the steady state is very long lived, and the disc continues to grow, this could explain the enormous intensity of novae-like A0620−00. If it fits among the less extreme mass ratios, the disc eccentricity is around 0.1–0.2, and a superhump should be observable with better photometry and a longer baseline (Smith et al. 2007). A0620−00 may also be at a transition between those cases, and its evolution might be somewhat more erratic, as suggested by the SMARTS data discussed earlier. For example, it may toggle between states of quiescence, superhumps and variability (like what we have observed here). It might, then, be erroneous to interpret this recent increase in brightness as the build towards outburst.

While we have strong evidence that the accretion disc around the black hole has grown out to the tidal distortion radius, evolved into an eccentric disc and started to precess, further study is required to verify our conclusion. Data from SMARTS, FLWO and *Spitzer* will further quantify flickering, and may reveal a superhump, or some new period consistent with our results, and future programs of tomography will track the evolution of the accretion disc. In anticipation of the impending outburst, and in light of progress in simulations, we suggest that this well-studied system not be disregarded or ignored, for it affords us the opportunity to watch the evolution of an accretion disc from quiescence to outburst, and the chance to test models for disc instabilities in X-ray novae.

ACKNOWLEDGMENTS

This research was supported by the NSF grant AST-0507637, the Harvard University Graduate School of Arts and Sciences (JN) and a SAO Clay Fellowship (DS). We wish to thank Cara Rakowski for help with the observations, Tom Marsh for use of his software packages, Jack Steiner for many useful discussions and the reviewer for a number of constructive comments which improved the quality of the paper.

REFERENCES

Elvis M., Griffiths C. G., Turner M. J. L., Page C., 1975, Int. Astron. Union Circ., 2184

Foulkes S. B., Haswell C. A., Murray J. R., Rolfe D. J., 2004, MNRAS, 349, 1179

Frank J., King A., Raine D., 2002, Accretion Power in Astrophysics. Cambridge Univ. Press, Cambridge
Friedman J. L., Ipser J. R., 1987, ApJ, 314, 594
Froning C. S., Robinson E. L., 2001, AJ, 121, 2212
Froning C. S., Robinson E. L., Bitner M. A., 2007, ApJ, 663, 1215
Gelino D. M., Harrison T. E., Orosz J. A., 2001, AJ, 122, 2668
Leibowitz E. M., Hemar S., Orio M., 1998, MNRAS, 300, L463
McClintock J. E., Remillard R. A., 1986, ApJ, 308, 110 (MR86)
McClintock J. E., Horne K., Remillard R. A., 1995, ApJ, 442, 358
Malaroda S., Levato H., Galliani S., 2001, VizieR On-line Data Catalog: III/216
Marsh T. R., 2001, in Boffin H. M. J., Steeghs D., Cuypers J., eds, LNP Vol. 573, Astrotomography: Indirect Imaging Methods in Observational Astronomy. Springer-Verlag, Berlin, p. 1
Marsh T. R., Horne K., Schlegel E. M., Honeycutt R. K., Kaitchuck R. H., 1990, ApJ, 364, 637
Marsh T. R., Robinson E. L., Wood J. H., 1994, MNRAS, 266, 137 (MRW94)
Paczynski B., 1971, ARA&A, 9, 183
Shahbaz T., Naylor T., Charles P. A., 1994, MNRAS, 268, 756
Shahbaz T., Hynes R. I., Charles P. A., Zurita C., Casares J., Haswell C. A., Araujo-Betancor S., Powell C., 2004, MNRAS, 354, 31 (S04)
Smith A. J., Haswell C. A., Murray J. R., Truss M. R., Foulkes S. B., 2007, MNRAS, 378, 785
Steeghs D., 2003, MNRAS, 344, 448
Steeghs D., Casares J., 2002, ApJ, 568, 273
Sterne T. E., 1941, Proc. Natl. Acad. Sci. USA, 27, 168
Wade R. A., Rucinski S. M., 1985, A&AS, 60, 471
Whitehurst R., King A., 1991, MNRAS, 249, 25

This paper has been typeset from a TEX/LATEX file prepared by the author.